JBIC Journal of Biological Inorganic Chemistry
https://doi.org/10.1007/s00775-019-01726-6

ORIGINAL PAPER

Bioinspired oxidation of oximes to nitric oxide with dioxygen by a nonheme iron(II) complex

Shrabanti Bhattacharya[1] · Triloke Ranjan Lakshman[1] · Subhankar Sutradhar[1] · Chandan Kumar Tiwari[1] · Tapan Kanti Paine[1]

Received: 18 April 2019 / Accepted: 24 September 2019

Abstract

The ability of two iron(II) complexes, [(Tp^{Ph2})Fe^{II}(benzilate)] (**1**) and [(Tp^{Ph2})(Fe^{II})$_2$(NPP)$_3$] (**2**) (Tp^{Ph2} = hydrotris(3,5-diphenylpyrazol-1-yl)borate, NPP-H = α-isonitrosopropiophenone), of a monoanionic facial N3 ligand in the O_2-dependent oxidation of oximes is reported. The mononuclear complex **1** reacts with dioxygen to decarboxylate the iron-coordinated benzilate. The oximate-bridged dinuclear complex (**2**), which contains a high-spin (Tp^{Ph2})Fe^{II} unit and a low-spin iron(II)–oximate unit, activates dioxygen at the high-spin iron(II) center. Both the complexes exhibit the oxidative transformation of oximes to the corresponding carbonyl compounds with the incorporation of one oxygen atom from dioxygen. In the oxidation process, the oxime units are converted to nitric oxide (NO) or nitroxyl (HNO). The iron(II)–benzilate complex (**1**) reacts with oximes to afford HNO, whereas the iron(II)–oximate complex (**2**) generates NO. The results described here suggest that the oxidative transformation of oximes to NO/HNO follows different pathways depending upon the nature of co-ligand/reductant.
Graphic abstract

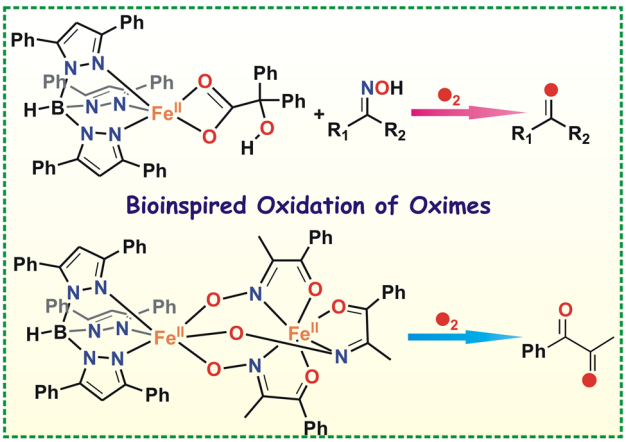

Keywords Oxidation · Oximes · Nitric oxide · Iron · Nonheme

Introduction

Nitric oxide (NO) acts as a bio-messenger [1] and governs many intracellular phenomena such as blood vessel dilation, neuronal signal transmission, cytotoxicity against pathogens and tumors, cellular respiration activity, etc. [2–8]. Investigations suggest that excess or lack of nitric oxide production

Electronic supplementary material The online version of this article (https://doi.org/10.1007/s00775-019-01726-6) contains supplementary material, which is available to authorized users.

✉ Tapan Kanti Paine
ictkp@iacs.res.in

[1] School of Chemical Sciences, Indian Association for the Cultivation of Science, 2A & 2B Raja S. C. Mullick Road, Jadavpur, Kolkata 700032, India

Published online: 21 October 2019

may cause diabetes, inflammation, myocardial ischemia and physiological imbalances [9–13]. Considering the biological and therapeutic importance of this small molecule, understanding of the biosynthesis route of nitric oxide has been the central focus of many investigations. Furthermore, nitroxyl (HNO), the one-electron reduced and protonated form of NO, has received attention in pharmacology and biology for its therapeutic potential [14–16].

Nitric oxide is generated from L-arginine in the reaction catalyzed by the heme monooxygenase, nitric oxide synthase (NOS) [17–20]. The structure of NOS reveals a redox active heme site similar to cytochrome P450 with the bound substrate and cofactor tetrahydrobiopterin (H4B) [21, 22]. In the first step of the reaction of NOS, L-arginine is converted to *N*-hydroxyarginine (NHA) by molecular oxygen [23–25]. In the subsequent step, 3-electron oxidation of NHA generates NO radical and L-citrulline (Scheme 1). In the reaction, one oxygen atom from molecular oxygen is incorporated into the hydroxylamine group of NHA, from which NO is formed [26, 27]. The first hydroxylation step is well-established for heme oxygenases, where an iron(IV)–oxo-porphyrin radical cation is involved as the active oxidant. However, the mechanistic details of the second step remain a matter of debate [28–30]. A nucleophilic iron(III)–hydroperoxide intermediate has been implicated to initiate the reaction via nucleophilic attack at the oxime carbon of NHA [31]. Inspired by the enzymatic reactions, simple substrates such as aldoximes/ketoximes have been used to generate NO in the reaction of iron–porphyrin complex with dioxygen [32, 33]. Based on model studies with iron(II)–porphyrin complexes, a radical-type autoxidation process involving oxidation of oximes to an iminoxyl radical intermediate has been proposed for NOS-catalyzed oxidation of NHA with O_2 [29]. An iron(III)–α-nitrosoalkylperoxide species, proposed as a key intermediate, eventually generated an iron(IV)–oxo complex, NO and L-citrulline. A (salen)Co^{II} complex has been reported to oxidize acetophenone oxime with *tert*-butylhydroperoxide in the presence of dioxygen. The oxidation reaction involves initial oxidation of the oxime to the corresponding iminoxy radical followed by the reaction with O_2 generating NO via a putative α-nitrosoalkylperoxo intermediate [34]. Therefore, similar to nitrites/nitrates and nitrosothiols, oximes can be used as precursors for NO and HNO generation [16, 35].

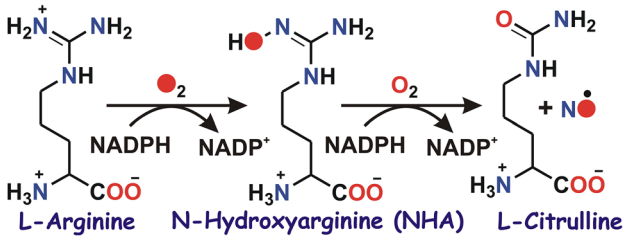

Scheme 1 Reactions catalyzed by nitric oxide synthase (NOS)

The enzyme, NOS not only utilizes tetrahydrobiopterin cofactor, but also receives electrons for the reductive activation of dioxygen and subsequent oxidation of NHA. With an objective to develop an understanding of the mechanism of the oxidation of oximes with dioxygen, we have explored the reactivity of a nonheme iron complex with metal-bound 2-electron reductant toward a series of oximes and of an iron(II)–oximate complex. We reported an iron(II)–benzilate complex, [(Tp^{Ph2})Fe^{II}(benzilate)] (**1**), of a monoanionic facial N3 ligand (Tp^{Ph2} = hydrotris(3,5-diphenylpyrazol-1-yl)borate) that reacted with dioxygen to display oxidative decarboxylation reactions. A nucleophilic iron–oxygen species was intercepted in the decarboxylation pathway. On the basis of mechanistic studies of the oxidation of different substrates by the iron(II)–benzilate complex and dioxygen, a nucleophilic iron(II)–hydroperoxide intermediate was proposed as the active oxidant [36–39]. Herein, we report the reactivity of the iron(II)–benzilate complex (**1**) toward different oximes in the presence of dioxygen (Chart 1). An iron(II)–oximate complex, [(Tp^{Ph2})(Fe^{II})$_2$(NPP)$_3$] (**2**) (NPP = α-isonitrosopropiophenone), was isolated and structurally characterized to compare its reactivity with **1**. The dioxygen reactivity of **2** along with the mechanistic studies on the oxidation of oximes by the iron complexes are presented in this work.

Chart 1 **a** Iron(II) complexes and **b** oximes used in this study

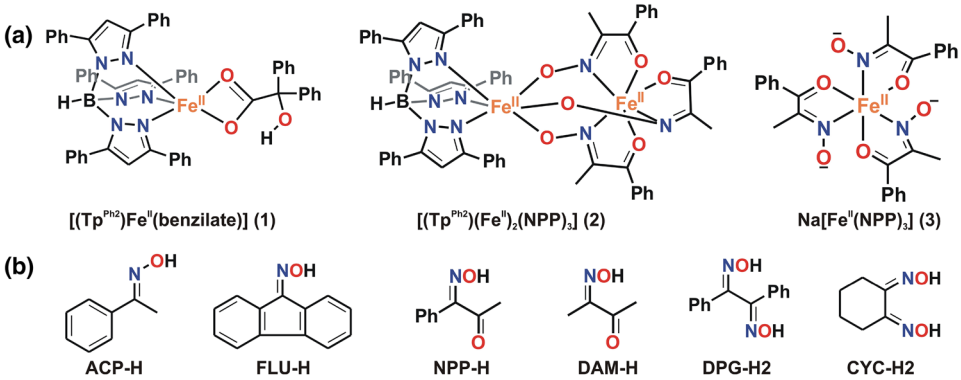

Materials and methods

Commercially available chemicals were used without further purification unless otherwise stated. Solvents were distilled and dried before use. Preparation and handling of air-sensitive compounds were carried out in an inert atmosphere glove box. Fourier transform infrared spectra were performed on a Shimadzu FT-IR 8400S instrument using KBr pellets. Elemental analyses were carried out on a Perkin Elmer 2400 series II CHN analyzer. UV–Vis spectra (single and time-dependent) were recorded on an Agilent 8453 diode array spectrophotometer. All room temperature NMR spectra were recorded on a Bruker Avance 500/300 MHz spectrometer and were referenced to residual deuterated solvents. X-band EPR spectra were collected on a JEOL JES-FA 200 instrument. GC–MS measurements were performed with a Perkin Elmer Clarus 600 instrument using an Elite 5 MS (30 m × 0.25 mm × 0.25 μm) column with a maximum temperature of 300 °C. Labeling experiments were carried out with the $^{18}O_2$ gas (99 atom%) and $H_2^{18}O$ from Icon Services Inc.

The KTp^{Ph2} ligand [40] and the iron complex **1** [36] were synthesized following the reported procedures. Although no problem was encountered during the synthesis of the complexes, perchlorate salts are potentially explosive and should be handled with care!

$[(Tp^{Ph2})Fe^{II}_2(NPP)_3]$ (2)

In a 50-mL round-bottomed flask, iron perchlorate hexahydrate (0.36 g, 1 mmol) was dissolved in 10 mL methanol. The ligand KTp^{Ph2} (0.35 g, 0.5 mmol) was added to the reaction mixture and was allowed to stir for 2–3 min. To the suspension was added a mixture of α-isonitrosopropiophenone (0.25 g, 1.5 mmol) and triethylamine (209 μL, 1.5 mmol in 1 mL of methanol) with constant stirring. The solution immediately turned blue, which was stirred for overnight under nitrogen environment. The reaction mixture was concentrated to dryness, the residue was dissolved in dichloromethane, and filtered. Evaporation of filtrate afforded blue microcrystalline solid. Crystals suitable for elemental analysis and X-ray diffraction were grown from a solvent mixture of dichloromethane and methanol. Yield: 0.485 g (76%). Anal. calcd for $C_{72}H_{58}BFe_2N_9O_6$ (1267.79 g/mol): C, 68.21; H, 4.61; N, 9.94. Found C, 68.44; H, 4.42; N, 10.42. IR (KBr, cm^{-1}): 3448 (br), 3059 (w), 2924 (w), 2619 (w), 1547 (w), 1479 (m), 1460 (m), 1331 (vs), 1285 (vs), 1175 (m), 1003 (m), 762 (m), 698 (vs). UV–Vis in benzene λ, nm (ε, M^{-1} cm^{-1}): 350 (3580), 680 (2000).

$Na[Fe^{II}(NPP)_3]$ (3)

Ammonium iron(II) sulfate hexahydrate (0.130 g, 0.3 mmol) was dissolved in 10 mL degassed water. To the solution, sodium salt of α-isonitrosopropiophenone (0.185 gm, 1 mmol) was added and stirred for 1 h. A deep blue solid precipitated, which was isolated by filtration and dried under vacuum. Yield: 0.19 g (67%). Anal. calcd for $C_{27}H_{24}FeN_3NaO_6$ (565.09 g/mol): C, 57.36; H, 4.28; N, 7.43. Found C, 57.02; H, 3.94; N, 7.39. IR (KBr, cm^{-1}): 3250 (br), 2924 (w), 1661 (vs), 1597 (m), 1452 (s), 1323 (s), 1184 (s), 1001 (vs), 897 (m), 712 (s), 665 (m). UV–Vis in dichloromethane λ, nm (ε, M^{-1} cm^{-1}): 336 (2480), 625 (1120).

Dioxygen reactivity

The iron(II) complex (0.02 mmol) was dissolved in dry benzene (10 mL). Bubbling O_2 gas through the solution of **1** and **2** resulted in a color change from blue to red for **2** and from colorless to green for **1**. The solution was allowed to stir at room temperature (15 min for **1** and 8 h for **2**). After the reaction, the solvent was evaporated to dryness and the residue was treated with 3 M HCl solution (10 mL). The organic products were extracted with diethyl ether (3 × 15 mL) and the organic layer was dried over anhydrous sodium sulfate. After removal of the solvent, the residue was analyzed by GC–MS and ^{1}H NMR spectroscopy. The reactions were performed in triplicate.

Reaction of complex 1 with oximes

Complex **1** (0.02 mmol) was dissolved in dry benzene (1 mL) under nitrogen atmosphere. To the solution was added the oxime (5 equiv) and pure oxygen gas was bubbled through the solution for 2 min. The reaction solution was allowed to stir for 20 min. After the reaction, the resulting solution was passed through a 15-cm silica (60–120 mesh size) column and washed with diethyl ether (10 mL). The organic phase was then analyzed by GC–MS and ^{1}H NMR spectroscopy. For GC analyses, naphthalene was used as an internal standard and the products were identified by comparison of their GC retention times and GC–MS with those of authentic compounds.

Control experiment

A control experiment was performed with iron(II) perchlorate hexahydrate (0.02 mmol) and oxime (1 mmol) in

dioxygen saturated benzene. No oxidized product of oxime was detected in the reaction solution.

^{1}H NMR (500 MHz, $CDCl_3$, 295 K) of organic products

Benzophenone: δ 7.80 (d, 4H), 7.59 (t, 2H), 7.50 (t, 4H); benzoic acid: δ 8.13 (d, 2H), 7.64 (t, 1H), 7.42 (t, 2H); benzil: δ 7.99 (d, 4H), 7.69 (t, 2H), 7.49 (t, 4H); 1-phenylpropane-1,2-dione: δ 7.89 (d, 2H), 7.73 (t, 1H), 7.64 (t, 2H), 2.17 (s, 3H); acetophenone: δ 7.94 (d, 2H), 7.64 (t, 1H), 7.56 (t, 2H), 2.5 (s, 3H).

Detection of nitric oxide

Nitric oxide (or HNO), formed in the reaction with iron(II) complexes, reacts with oxygen and water to form nitrous acid which is quantitatively converted to a diazonium salt by reaction with sulfanilic acid (Griess B) in acid solution. The diazonium salt is then coupled to *N*-(1-naphthyl)ethylenediamine (Griess A), forming an azo dye that can be spectrophotometrically quantified based on its absorbance at 548 nm [41, 42].

Reaction of the complexes (1 and 2) with triphenylphosphine

A mixture of the iron(II) complex **1** (0.04 mmol) and oxime (0.2 mmol) (or iron(II) complex only for **2**) was taken in a Schlenk tube. To the mixture was added oxygen saturated benzene (1 mL) by a syringe and the reaction flask was closed fully to avoid loss of HNO/NO from the solution. After 20 min of stirring, triphenylphosphine (0.08 mmol) dissolved in benzene (500 µL) was added by a syringe. The reaction solution was allowed to stir for 24 h and passed through a 15-cm silica (60–120 mesh) column and washed with diethyl ether (10 mL). The dark-green solution was dried under vacuum and was analyzed by ^{31}P NMR spectroscopy using H_3PO_4 as a standard. For the detection of NO and HNO, the method reported by King and co-workers were followed [43]. In the reaction with complex **1** and oxime, the resonances for aza-ylide and triphenylphosphine oxide appear at 18.1 ppm and 28.6 ppm, respectively. For complex **2**, the resonance for triphenylphosphine oxide appears at 27.0 ppm. Resonance signal for triphenylphosphine from the reaction with **1** and oxime appears at −4.2 ppm, whereas it appears at −5.7 ppm for complex **2**.

X-ray crystallographic data collection and refinement and solution of the structure

X-ray single crystal data of **2** was collected using Mo Kα (λ = 0.7107 Å) radiation on a SMART APEX diffractometer equipped with charge-coupled device (CCD) area detector. Data collection, data reduction and structure solution/refinement were performed using the APEX II software package [44]. The structure of the complex was solved by intrinsic method and refined by the full-matrix least-squares method based on F^2 with all observed reflections. All the non-hydrogen atoms were treated anisotropically. At the end of the refinement cycles, some disordered electron densities were located in the asymmetric unit. SQUEEZE calculations indicated the presence of 71 electrons per unit cell [45]. Crystallographic data for the complex are summarized in Table S1.

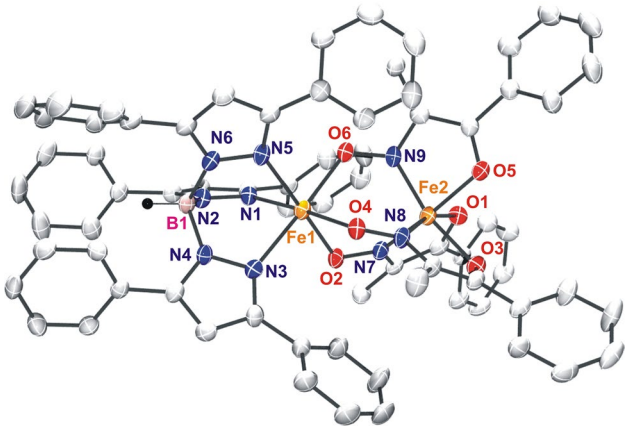

Fig. 1 ORTEP plot of complex **2** with 40% thermal ellipsoid parameters. All hydrogen atoms except that on B have been omitted for clarity. Average distances: Fe1–N = 2.209 Å, Fe2–N = 1.89 Å, Fe1–O = 2.095 Å and Fe2–O = 1.953 Å

Results and discussion

Synthesis and characterization

Complex **1** was prepared following the protocol reported earlier by our group, [36] while the dimeric complex **2** was isolated from the reaction of KTp^{Ph2}, iron(II) perchlorate hydrate and a basic solution of α-isonitrosopropiophenone (NPP-H) in methanol under nitrogen atmosphere (see Experimental section). The ^{1}H NMR spectrum of **2** in $CDCl_3$ shows paramagnetically shifted resonances indicating the presence of high-spin iron(II) center in the complex (Fig. S1). The blue solution of complex **2** exhibits intense and broad bands at 494 nm, 590 nm and 680 nm, attributable to Fe(II)-to-nitroso charge-transfer (CT) transitions (Fig. S3) [46]. Similar CT bands are been observed in the tris(oximato)iron(II) complex $Na[Fe(NPP)_3]$ (**3**) (Experimental and Fig. S3). It is important to mention here that complex **3** displays proton resonances in the region between 0 ppm and 8 ppm typical of low-spin iron(II) complex (Fig. S2).

The composition of the complex and the binding mode of the monoanionic oxime were established by single crystal X-ray structure of **2** (Fig. 1). The structure of the dimeric complex reveals that one of the iron centers (Fe1) is ligated by the three nitrogen donors from the facial tridentate ligand and three oxygen donors from the NPP anion. The other iron center (Fe2) is coordinated by the three nitrogens and three oxygens from oximate anions. Two iron centers in the complex are bridged by three oximate groups. The absence of counter anion confirms the neutral nature of the complex. Three nitrogen donors of the supporting ligand form the iron–nitrogen(pyrazole) bonds that are longer than those formed through the coordination of oxime nitrogens. The average Fe1–N bond length is closely comparable with that of the high-spin iron(II) complexes of Tp^{Ph2} ligand, whereas the average Fe2–N bond distance reveals the low-spin iron(II) center (Table S2) [47, 48]. The oximate oxygen binds to the iron center trans to the pyrazole nitrogen donors with the N5–Fe1–O2, N1–Fe1–O4 and N3–Fe1–O6 bond angles of 174.90°, 176.12° and of 175.09°, respectively.

Reactivity of the complexes

Complex **1** has been reported to react with O_2 in benzene exhibiting quantitative decarboxylation of benzilate to benzophenone over a period of 20 min at 298 K. The O_2-derived metal-based oxidant can be intercepted by different substrates, [36] including a variety of oximes investigated in this work (Scheme 2). The paramagnetically shifted proton resonances of **1** in the NMR spectrum slowly disappear yielding a spectrum typical of a diamagnetic species after 15 min of reaction with oximes (Fig. S4). To verify the product from the N–OH group of oxime, triphenylphosphine (Ph_3P) was reacted with the iron(II)–benzilate complex in the presence of NPP-H and dioxygen. ^{31}P NMR analyses clearly indicate the formation of triphenylphosphine oxide (Ph_3P=O) and aza-ylide (Ph_3P=NH) from triphenylphosphine (Fig. 2a) [43, 49]. The peak positions for Ph_3P and Ph_3PO in case of complex **1** are slightly downfield shifted likely due to non-covalent interactions with the Ph_3P=NH present in the solution. The control experiment with complex **1** and Ph_3P reveals formation of no such products. The presence

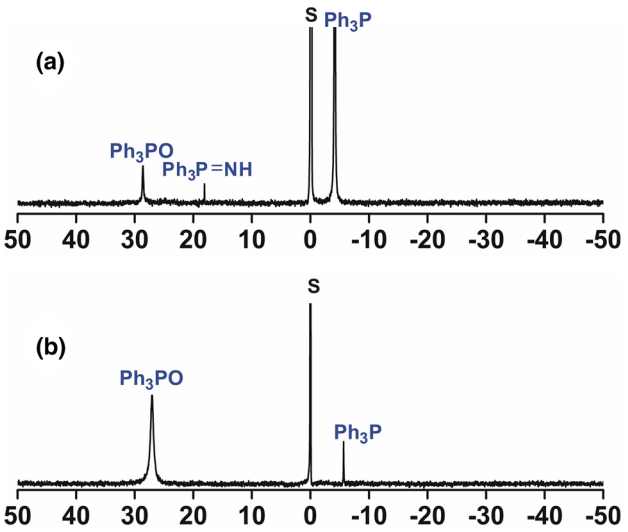

Fig. 2 ^{31}P NMR spectra of the triphenylphosphine-derived product after the reaction **a** with complex **1** and α-isonitrosopropiophenone (in DMSO-d_6) and **b** with complex **2** (in DMSO-d_6). The peaks are referenced to H_3PO_4 (indicated as "S")

Scheme 2 Oxidation of oximes with O_2 by complex **1**

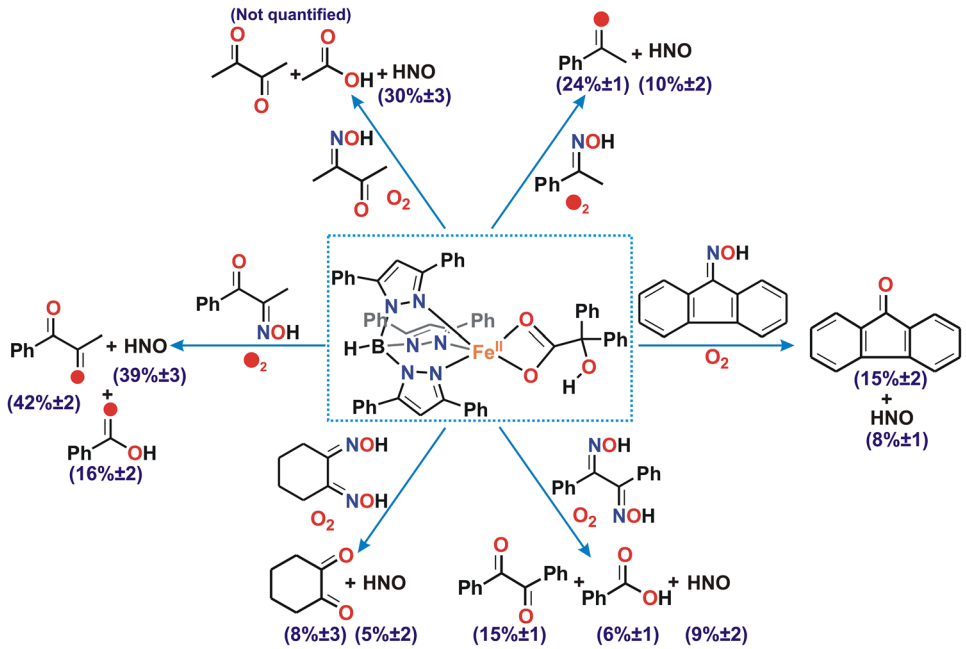

of resonance signal for aza-ylide in the ^{31}P NMR spectrum indicates the formation of HNO in the reaction between **1** and oxime. However, this can only be definitely proven by ^{15}N labeling studies.

Analysis of organic products after the reaction reveals that aromatic oximes are oxidatively cleaved by complex **1** to afford the corresponding carbonyl compounds and nitroxyl (Scheme 2). While NO and HNO were detected by ^{31}P NMR spectroscopy, their quantification was performed by Griess assay [41, 42]. Acetophenone oxime (ACP-H, 5 equiv) affords acetophenone (24%) and HNO (10%) (Fig. S5). Fluorenone oxime (FLU-H, 5 equiv) reacts with complex **1** and dioxygen to form fluorenone (15%) and HNO (8%) (Fig. S6). With diacetylmonooxime (DAM-H, 5 equiv), HNO is detected to an extent of 30%. The reaction of **1** with NPP-H (5 equiv) yields 1-phenylpropane-1,2-dione (42%) along with HNO (39%) (Fig. S7). It is important to mention here that Griess assay is an indirect method for the quantification of HNO/NO due to the interference of nitrite ion generated in situ in the reaction with O_2. As a result, there remains a mismatch between the percentage yield of ketone and HNO. In the reaction, 16% benzoic acid is also detected. Interestingly, when complex **1** is allowed to react with benzil under oxygen environment, benzoic acid (12%) is observed as a cleavage product. Thus, benzoic acid is formed from the diketone product [50]. Isotope labeling studies with $^{16}O_2$ and $H_2^{18}O$ confirm the incorporation of the labeled oxygen atom into benzoic acid (Fig. S8). These results are in agreement with the involvement of an iron–oxygen species that exchanges its oxygen atom with water in the reaction pathway. Thus, in the reaction with NPP-H, 42% of the active oxidant is involved in converting NPP to the corresponding diketone and the rest of the oxidant cleaves the C–C bond of diketone to form the carboxylic acid.

To assess the source of the oxygen atom of the organic products, $^{18}O_2$ labeling experiment was conducted with complex **1** and ACP-H. The GC-mass spectrum of the oxidized solution shows about 62% incorporation of one oxygen atom into acetophenone (Fig. 3). A mixed labeling experiment with O_2 and $H_2^{18}O$ confirms no incorporation of labeled oxygen atom into the ketone product.

The reactivity of **1** toward dioximes was also investigated. Diphenylglyoxime (DPG-H2, 5 equiv) forms a mixture of benzil (15%) and benzoic acid (6%) (Fig. S9). In the reaction, 9% of HNO is detected. When cyclohexane-1,2-dioxime (CYC-H2) is treated with complex **1** and O_2, 1,2-cyclohexanedione (8%) is obtained as the sole product along with HNO (5%) (Fig. S10). It was reported that complex **1** reacted with oxygen in the absence of any external substrate to hydroxylate one of the phenyl rings of Tp^{Ph2} to an extent of 90% exhibiting a broad charge-transfer band at 600 nm [36]. In the oxidation of oximes by **1** and O_2, the CT band shifts to 500 nm. The shifting of the absorbance

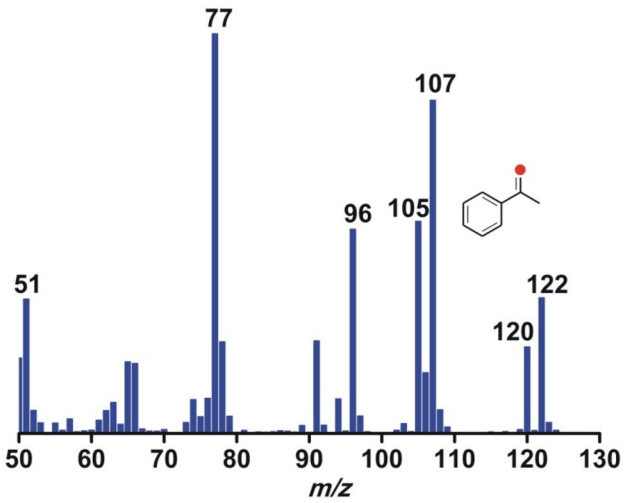

Fig. 3 GC-mass spectrum of acetophenone formed in the reaction of **1** with acetophenone oxime (5 equiv) and $^{18}O_2$

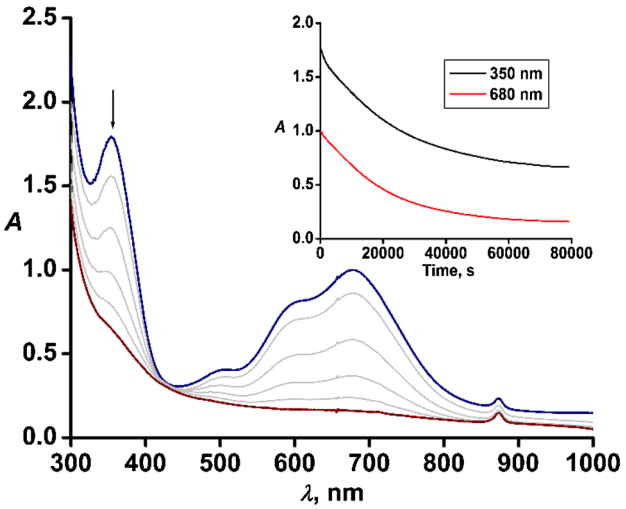

Fig. 4 Optical spectral changes of the iron complex **2** (0.5 mM in benzene) during the reaction with dioxygen at 298 K

maxima from 600 to 500 nm is possibly caused due to the coordination of the excess oxime to the iron(III) center of the oxidized complex (Fig. S11).

Complex **2** is stable in solution under a nitrogen environment, but is reactive toward dioxygen. The CT bands of **2** slowly decay upon exposure of a benzene solution of the complex to dioxygen (Fig. 4). After stirring the solution of complex **2** in O_2-saturated benzene for 8 h, the reaction products were isolated by acid work-up. The ^{1}H NMR spectrum reveal that 1-phenyl-1,2-propanedione (29%) and benzoic acid (6%) are formed (Fig. S12). ^{31}P NMR spectroscopy reveals the formation of Ph_3PO from Ph_3P, supporting the generation of NO (28%) from **2** (Fig. 2b) [49]. It is important

to mention here that neither the diketone nor the carboxylic acid product is formed from complex **2** in the absence of dioxygen. The labeling experiment with $^{18}O_2$ demonstrates the shift of the ion peak at *m/z* 148 to *m/z* 150 confirming the incorporation of one labeled oxygen atom into 1-phenyl-1,2-propanedione (Fig. 5). The ion peak of the other product, benzoic acid, also shifts to *m/z* 124 from *m/z* 122 (Fig. S13a). Of note, 1-phenyl-1,2-propanedione does not contain any labeled oxygen atom from water (Fig. S13b). These data strongly implicate the involvement of an iron–oxygen intermediate which does not exchange its oxygen with water in the reaction pathway. It is important to mention that less than 2% NO is detected in the reaction of **3** with dioxygen (Fig. S14). These results support that the low-spin tris(oximato) Fe^{II} center in **2** does not participate in O_2 activation reaction.

Based on the results discussed above, mechanistic proposals for the oxidative transformation of oximes by **1** and **2** are put forward. The two complexes follow distinct different pathways affording nitric oxide or nitroxyl (Scheme 3). Although no iron–oxygen intermediate species was observed experimentally, it is proposed that an iron(III)–superoxo species is initially generated from both the complexes. Reduction of the superoxide unit by electron transfer from the iron-coordinated benzilate in **1** results in the formation of a putative iron(II)–(hydro)peroxo species (**I**). It has been reported earlier that the iron–oxygen species from **1** exhibits nucleophilic character and therefore it has a tendency to attack the electrophilic centers of substrates such as aldehydes and α-hydroxy ketones [50]. In analogy with the reactivity with electrophilic substrates, intermediate **I** is proposed to attack the carbon atom of oxime group. The peroxo-iron(II) intermediate (**II**) thus formed then undergoes heterolytic O–O bond cleavage affording carbonyl compound, HNO and iron(II)–hydroxide species (**III**).

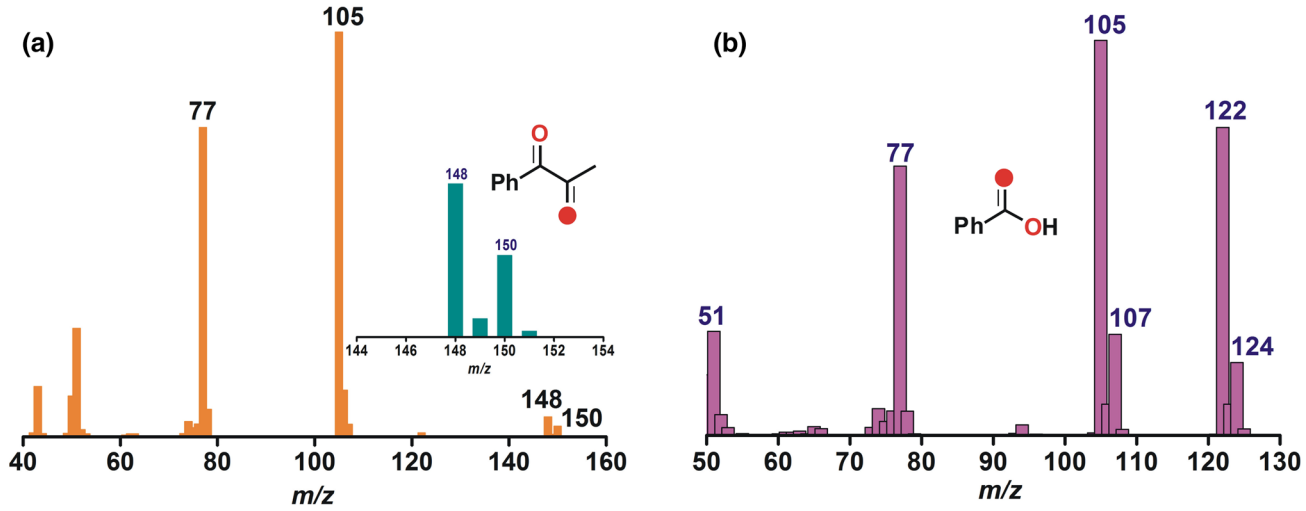

Fig. 5 GC-mass spectra of **a** 1-phenylpropane-1,2-dione and **b** benzoic acid formed in the reaction of **2** with $^{18}O_2$

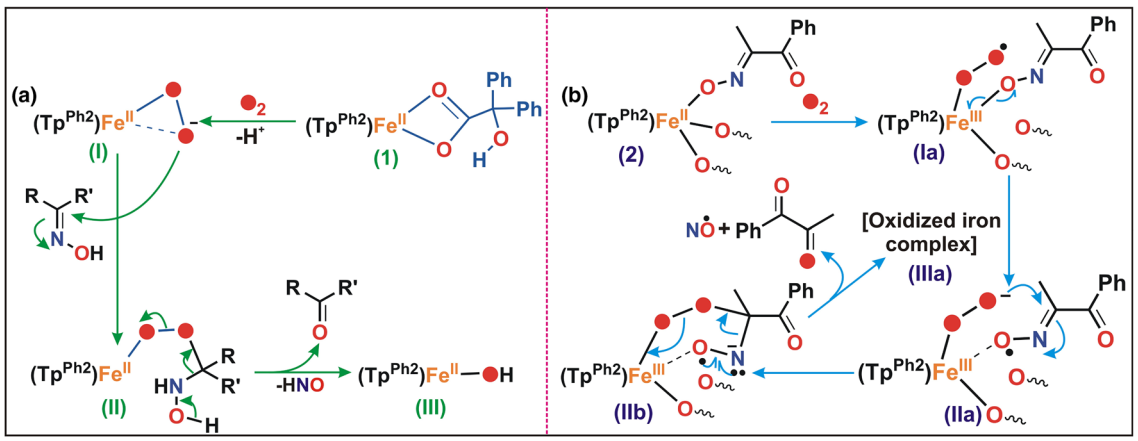

Scheme 3 Mechanistic proposals of the oxidative conversion of oxime to nitric oxide by the iron(II) complexes

For complex **2**, dioxygen activation takes place at the high-spin iron site upon decoordination of one of the oximates. The iron(III)–superoxide species (**Ia**) thus generated is reduced by one electron from one of the coordinated oximates with subsequent formation of a metal-bound iminoxyl radical (**IIa**). Intermediate **IIa** then rearranges to form a peroxo (iron)–nitroso species (**IIb**), which then undergoes O–O cleavage to afford an iron(III)–hydroxide product (**IIIa**), 1,2-diketone and NO.

Conclusion

In conclusion, we have investigated the activity of a non-heme iron(II)–benzilate complex of a tris(pyrazolyl) borate ligand in the oxidation of series of oximes with dioxygen. The reactivity of the complex was compared to that of an iron(II)–oximate complex of the same ligand. Both the complexes oxidize oximes to the corresponding carbonyl compounds with concomitant formation of nitric oxide but in different redox states. While the reactions of the iron(II)–benzilate complex with oximes afford HNO, the iron(II)–oximate complex yields NO radical. Isotope labeling experiments establish that the oxygen atom of carbonyl compound is derived from O_2. It is proposed that the reaction involves an iron(III)–superoxide species, which diverges into two different pathways depending upon the nature of co-ligand. Benzilate provides two electrons for dioxygen reduction on the iron center with the formation of HNO, whereas the iron(II)–oximate complex lacks the reducing equivalents leading to the formation of NO. In spite of the differences in the structures, the iron complexes discussed here display reactivity reminiscent of the heme enzyme, NOS.

Acknowledgements TKP acknowledges Science and Engineering Research Board (SERB), India, for the financial support (Project: EMR/2014/000972). SB thanks the Department of Science and Technology (DST), Govt. of India, for INSPIRE fellowship, and TRL thanks the Council of Scientific and Industrial Research (CSIR), India, for a research fellowship.

References

1. Dangl J (1998) Nature 394(525):527
2. Murad F (1999) Angew Chem Int Ed 38:1856–1868
3. Ignarro LJ (1999) Angew Chem Int Ed 38:1882–1892
4. Hansen MB, Dresner LS, Wait RB (1998) Physiol Res 47:307–327
5. Agnihotri N, Lopez-Garcia JC, Hawkins RD, Arancio O (1998) Histol Histopathol 13:1155–1162
6. Albina JE, Reichner JS (1998) Cancer Metastasis Rev 17:39–53
7. Brown GC (1999) Biochim Biophys Acta Bioenerg 1411:351–369
8. Terasaka E, Yamada K, Wang P-H, Hosokawa K, Yamagiwa R, Matsumoto K, Ishii S, Mori T, Yagi K, Sawai H, Arai H, Sugimoto H, Sugita Y, Shiro Y, Tosha T (2017) Proc Natl Acad Sci USA 114:9888–9893
9. Rask-Madsen C, King GL (2007) Nat Clin Pract Endocrinol Metab 3:46–56
10. Shah NS, Billiar TR (1998) Environ Health Perspect Suppl 106:1139–1143
11. Suzuki A, Kudoh S, Mori K, Takahashi N, Suzuki T (2004) Int J Urol 11:837–844
12. Hammerman C, Kaplan M (1998) Clin Perinatol 25:757–777
13. Cosentino F, Luscher TF (1998) J Cardiovasc Pharmacol 32:S54–S61
14. Paolocci N, Jackson MI, Lopez BE, Miranda K, Tocchetti CG, Wink DA, Hobbs AJ, Fukuto JM (2007) Pharmacol Ther 113:442–458
15. Irvine JC, Ritchie RH, Favaloro JL, Andrews KL, Widdop RE, Kemp-Harper BK (2008) Trends Pharmacol Sci 29:601–608
16. Miao Z, King SB (2016) Nitric Oxide 57:1–14
17. Daff S (2010) Nitric Oxide 23:1–11
18. Foerstermann U, Sessa WC (2012) Eur Heart J 33:829–837
19. Knowles RG, Moncada S (1994) Biochem J 298:249–258
20. Agapie T, Suseno S, Woodward JJ, Stoll S, Britt RD, Marletta MA (2009) Proc Natl Acad Sci USA 106:16221–16226
21. Bredt DS, Hwang PM, Glatt CE, Lowenstein C, Reed RR, Snyder SH (1991) Nature 351:714–718
22. Crane BR, Arvai AS, Ghosh DK, Wu C, Getzoff ED, Stuehr DJ, Tainer JA (1998) Science 279:2121–2126
23. Boggs S, Huang L, Stuehr DJ (2000) Biochemistry 39:2332–2339
24. Stuehr DJ, Kwon NS, Nathan CF, Griffith OW, Feldman PL, Wiseman J (1991) J Biol Chem 266:6259–6263
25. Campos KL, Giovanelli J, Kaufman S (1995) J Biol Chem 270:1721–1728
26. Leone AM, Palmer RMJ, Knowles RG, Francis PL, Ashton DS, Moncada S (1991) J Biol Chem 266:23790–23795
27. Korth HG, Sustmann R, Thater C, Butler AR, Ingold KU (1994) J Biol Chem 269:17776–17779
28. Bec N, Gorren ACF, Voelker C, Mayer B, Lange R (1998) J Biol Chem 273:13502–13508
29. Wang CCY, Ho DM, Groves JT (1999) J Am Chem Soc 121:12094–12103
30. Marletta MA (1993) J Biol Chem 268:12231–12234
31. Woodward JJ, Chang MM, Martin NI, Marletta MA (2009) J Am Chem Soc 131:297–305
32. Groves JT, Wang CCY (1997) FASEB J 11:A769–A1458
33. Groves JT, Wang CCY (2000) Curr Opin Chem Biol 4:687–695
34. Nishinaga A, Yamazaki S, Miwa T, Matsuura T (1991) React Kinet Catal Lett 43:273–276
35. Sha X, Isbell TS, Patel RP, Day CS, King SB (2006) J Am Chem Soc 128:9687–9692
36. Paria S, Que L, Paine TK (2011) Angew Chem Int Ed 50:11129–11132
37. Paria S, Chatterjee S, Paine TK (2014) Inorg Chem 53:2810–2821
38. Chatterjee S, Paine TK (2015) Angew Chem Int Ed 54:9338–9342
39. Chatterjee S, Paine TK (2016) Angew Chem Int Ed 55:7717–7722
40. Kitajima N, Fujisawa K, Fujimoto C, Morooka Y, Hashimoto S, Kitagawa T, Toriumi K, Tatsumi K, Nakamura A (1992) J Am Chem Soc 114:1277–1291
41. Feelisch M, Schoenafinger K, Noack E (1992) Biochem Pharmacol 44:1149–1157
42. Miranda KM, Espey MG, Yamada K, Krishna M, Ludwick N, Kim S, Jourd'heuil D, Grisham MB, Feelisch M, Fukuto JM, Wink DA (2001) J Biol Chem 276:1720–1727
43. Reisz JA, Klorig EB, Wright MW, King SB (2009) Org Lett 11:2719–2721
44. Dong Y, Fujii H, Hendrich MP, Leising RA, Pan G, Randall CR, Wilkinson EC, Zang Y, Que L Jr, Fox BG, Kauffmann K, Münck E (1995) J Am Chem Soc 117:2778–2792
45. Van der Sluis P, Spek AL (1990) Acta Crystallogr Sect A Found Crystallogr A46:194–201

46. Gerasimchuk NN, Domasevich KV (1992) Zhurnal Neorganicheskoi Khimii 37:2245–2252
47. Mehn MP, Fujisawa K, Hegg EL, Que L Jr (2003) J Am Chem Soc 125:7828–7842
48. Paine TK, Zheng H, Que L Jr (2005) Inorg Chem 44:474–476
49. Rhine MA, Rodrigues AV, Urbauer RJB, Urbauer JL, Stemmler TL, Harrop TC (2014) J Am Chem Soc 136:12560–12563
50. Bhattacharya S, Rahaman R, Chatterjee S, Paine TK (2017) Chem Eur J 23:3815–3818